ISSN 1995-0802, Lobachevskii Journal of Mathematics, 2018, Vol. 39, No. 7, pp. 874–883. © Pleiades Publishing, Ltd., 2018.

Grid-Characteristic Numerical Method for Low-Velocity Impact Testing of Fiber-Metal Laminates

K. A. Beklemysheva[1*], A. V. Vasyukov[1], A. O. Kazakov[1***], and I. B. Petrov[1****]**

(Submitted by A. V. Lapin)

[1] *Moscow Institute of Physics and Technology, Institutskii per. 9, Dolgoprudnyi, Moscow oblast, 141701 Russia*

Received December 4, 2017

Abstract—The grid-characteristic numerical method (GCM) for hyperbolic equations systems is applied in many science fields—gas dynamics, hydrodynamics, plasma dynamics, etc. Its application for problems of dynamics of deformable solids is less popular, especially in comparison with finite elements methods. GCM shows good results and high performance for elastic wave problems in the approximation of small deformations—seismic survey and ultrasound non-destructive testing in medicine, aviation and railway industry. Low-velocity impacts (hail, dropped tool, bird strike, etc.) are one of the most dangerous load types for polymer composites. They cause barely visible impact damage (BVID) that can only be detected by a thorough ultrasound testing, but severely reduces the residual strength of the material, especially for a compression load along the surface. This testing increases the operating cost, and its necessity can be easily missed, which greatly reduces the reliability of polymer composites. Hybrid fiber-metal composites (GLARE, ARALL, titanium composite laminates) were developed to unify the advantageous properties of polymer composites and metal. The addition of a thin metal layer (1–2 mm) helps to reduce the impact vulnerability of polymer composites in case of a penetration or significant deformations of the material. The application of GCM for low-velocity impact problems can help to explain the damage pattern in fiber-metal composites in case of low-velocity strike, including delamination effects, by modelling elastic wave processes in the complex anisotropic medium. This article contains the brief description of the GCM and numerical results that were obtained for model problems of a low-velocity impact on titanium composite laminates.

DOI: 10.1134/S1995080218070065

Keywords and phrases: *Grid-characteristic method, fiber-metal laminates, low-velocity impact, delamination.*

1. INTRODUCTION

Low-velocity impacts (LVI) often occur during the maintenance of composite parts—hail, dropped tool, bird strike, etc. They cause barely visible impact damage (BVID, [1]) that can only be detected by a thorough ultrasound testing, but severely reduces the residual strength of the material (up to 50%, according to [2]), especially for a compression load along the surface. This testing increases the operating cost, and its necessity can be easily missed, which greatly reduces the reliability of polymer composites.

The term LVI was widely accepted for this kind of impacts, because in experimental setups with the standart drop-weight tool the BVID effects are achieved on low impact velocities—from 5 to 100 m/s [1, 3, 4], depending on material, plate thickness, striker shape etc. The same BVID effects can occur

*E-mail: amisto@yandex.ru
**E-mail: vasyukov@gmail.com
***E-mail: alexanderkazak@yandex.ru
****E-mail: petrov@mipt.ru

with a light striker falling with a high speed, so the striker energy is considered to be a better impact parameter [5, 6].

Hybrid fiber-metal composites (GLARE, ARALL, titanium composite laminates) were developed to unify the advantageous properties of polymer composites and metal [7]. The addition of a thin metal layer (1–2 mm) helps to reduce the strike vulnerability of polymer composites in case of a penetration or significant deformations of the material. Thorough reviews with chronological order can be found in [8] and [9]. Many numerical and experimental studies are focused on fiber-metal laminates, but most of them consider penetration and significant deformations and do not deal with low-velocity strike in its original problematic statement.

The modelling of composite destruction is a pressing problem both for mathematics and mechanics. The international project WWFE (World Wide Failure Exercise), entirely devoted to the simulation of the failure of polymeric composition materials (PCMs), reinforced by long fibers, showed that the theory of the failure of composites is far from being complete [10, 11]. This series of projects unites the leading research teams all over the world, providing a standartized testing ground for various composite destruction criteria. After analysing the results of a full-scale experiment in WWFE II, it was concluded that the existing criteria do not have a sufficiently reliable prediction ability concerning direct engineering applications. The set of criteria used in this work (Tsai–Hill, Tsai–Wu, Drucker–Prager, Hashin, Puck) was chosen [12] because these criteria are widely applied in commercial software packages and use a limited set of material parameters, availaible in open access.

GCM shows good results and high performance for elastic wave problems in the approximation of small deformations—seismic survey [13] and ultrasound non-destructive testing in medicine [14], aviation [15] and railway industry [16]. It allows for a simple and transparent statement of contact and border conditions, including consuming border and destructible contact. The finite elements method that is commonly used for dynamics of deformable solids is reported to have certain problems with oscillations on the destructible contact [17]. The application of GCM for low-velocity impact problems can help to explain the damage pattern in composites, including delamination effects, by modelling elastic wave processes in the complex anisotropic medium.

This article contains the brief description of the GCM and numerical results that were obtained for model problems of a low-velocity impact on titanium composite laminates.

2. GOVERNING EQUATIONS

Generally, the linear dependence between stress and deformation i n elastic medium is described as follows [18]: $C_{ijkl} = \partial\sigma_{ij}/\partial\varepsilon_{kl}$, where σ_{ij} is the stress tensor, $\partial\varepsilon_{kl}$ is the deformation tensor, C_{ijkl} is the elastic properties tensor. In the three-dimensional case C_{ijkl} has $3^4 = 81$ components, but not all of them are independent. Deformation and stress tensors are symmetric [19], and it reduces the amount of independent parameters to 36. Considering w as an elastic potential: $dw = \sigma_{ij} d\varepsilon_{ij}$, $C_{ijkl} = \frac{\partial^2 w}{\partial\varepsilon_{ij}\varepsilon_{kl}}$. Since the derivative calculation order does not affect the result, we see an additional symmetric property: $C_{ijkl} = C_{klij}$. The amount of independent parameters reduces to 21.

For practical usage, the tensor C_{ijkl} is usually rewritten as a matrix c_{ij}. Thus, the mathematical model of a three-dimensional elastic anisotropic medium can be described by the following system of equations [19]:

$$\frac{\partial v_x}{\partial t} = \frac{1}{\rho}\left(\frac{\partial\sigma_{xx}}{\partial x} + \frac{\partial\sigma_{xy}}{\partial y} + \frac{\partial\sigma_{xz}}{\partial z}\right), \quad \frac{\partial v_y}{\partial t} = \frac{1}{\rho}\left(\frac{\partial\sigma_{xy}}{\partial x} + \frac{\partial\sigma_{yy}}{\partial y} + \frac{\partial\sigma_{yz}}{\partial z}\right),$$

$$\frac{\partial v_z}{\partial t} = \frac{1}{\rho}\left(\frac{\partial\sigma_{xz}}{\partial x} + \frac{\partial\sigma_{yz}}{\partial y} + \frac{\partial\sigma_{zz}}{\partial z}\right),$$

$$\frac{\partial\sigma_{xx}}{\partial t} = c_{11}\frac{\partial v_x}{\partial x} + c_{12}\frac{\partial v_y}{\partial y} + c_{13}\frac{\partial v_z}{\partial z} + c_{14}\left(\frac{\partial v_z}{\partial y} + \frac{\partial v_y}{\partial z}\right) + c_{15}\left(\frac{\partial v_z}{\partial x} + \frac{\partial v_x}{\partial z}\right) + c_{16}\left(\frac{\partial v_y}{\partial x} + \frac{\partial v_x}{\partial y}\right),$$

$$\frac{\partial\sigma_{yy}}{\partial t} = c_{12}\frac{\partial v_x}{\partial x} + c_{22}\frac{\partial v_y}{\partial y} + c_{23}\frac{\partial v_z}{\partial z} + c_{24}\left(\frac{\partial v_z}{\partial y} + \frac{\partial v_y}{\partial z}\right) + c_{25}\left(\frac{\partial v_z}{\partial x} + \frac{\partial v_x}{\partial z}\right) + c_{26}\left(\frac{\partial v_y}{\partial x} + \frac{\partial v_x}{\partial y}\right),$$

$$\frac{\partial\sigma_{zz}}{\partial t} = c_{13}\frac{\partial v_x}{\partial x} + c_{23}\frac{\partial v_y}{\partial y} + c_{33}\frac{\partial v_z}{\partial z} + c_{34}\left(\frac{\partial v_z}{\partial y} + \frac{\partial v_y}{\partial z}\right) + c_{35}\left(\frac{\partial v_z}{\partial x} + \frac{\partial v_x}{\partial z}\right) + c_{36}\left(\frac{\partial v_y}{\partial x} + \frac{\partial v_x}{\partial y}\right),$$

$$\frac{\partial \sigma_{yz}}{\partial t} = c_{14}\frac{\partial v_x}{\partial x} + c_{24}\frac{\partial v_y}{\partial y} + c_{34}\frac{\partial v_z}{\partial z} + c_{44}\left(\frac{\partial v_z}{\partial y} + \frac{\partial v_y}{\partial z}\right) + c_{45}\left(\frac{\partial v_z}{\partial x} + \frac{\partial v_x}{\partial z}\right) + c_{46}\left(\frac{\partial v_y}{\partial x} + \frac{\partial v_x}{\partial y}\right),$$

$$\frac{\partial \sigma_{xz}}{\partial t} = c_{15}\frac{\partial v_x}{\partial x} + c_{25}\frac{\partial v_y}{\partial y} + c_{35}\frac{\partial v_z}{\partial z} + c_{45}\left(\frac{\partial v_z}{\partial y} + \frac{\partial v_y}{\partial z}\right) + c_{55}\left(\frac{\partial v_z}{\partial x} + \frac{\partial v_x}{\partial z}\right) + c_{56}\left(\frac{\partial v_y}{\partial x} + \frac{\partial v_x}{\partial y}\right),$$

$$\frac{\partial \sigma_{xy}}{\partial t} = c_{16}\frac{\partial v_x}{\partial x} + c_{26}\frac{\partial v_y}{\partial y} + c_{36}\frac{\partial v_z}{\partial z} + c_{46}\left(\frac{\partial v_z}{\partial y} + \frac{\partial v_y}{\partial z}\right) + c_{56}\left(\frac{\partial v_z}{\partial x} + \frac{\partial v_x}{\partial z}\right) + c_{66}\left(\frac{\partial v_y}{\partial x} + \frac{\partial v_x}{\partial y}\right), \tag{1}$$

where ρ is the density, v_x, v_y, v_z are deformation velocity vector components, σ_{xx}, σ_{xy}, σ_{yy}, σ_{yz}, σ_{zz} are stress tensor components, c_{ij} is the elastic properties matrix.

Considering $\vec{u} = \{v_x, v_y, v_z, \sigma_{xx}, \sigma_{xy}, \sigma_{xz}, \sigma_{yy}, \sigma_{yz}, \sigma_{zz}\}^T$, system of equations (1) can be rewritten as follows:

$$\frac{\partial \vec{u}}{\partial t} + \mathbf{A}_x\frac{\partial \vec{u}}{\partial x} + \mathbf{A}_y\frac{\partial \vec{u}}{\partial y} + \mathbf{A}_z\frac{\partial \vec{u}}{\partial z} = 0, \tag{2}$$

where $\mathbf{A}_x$, $\mathbf{A}_y$, $\mathbf{A}_z$ are rheological matrixes that correspond to the original system (1). Another simplification of the elastic properties matrix comes from the material under consideration. Most composites can be described as orthorhombic anisotropic materials—they have three mutually perpendicular symmetry planes, and their elastic parameters differ in three mutually perpendicular directions.

For an orthorhombic material the amount of independent components in elastic properties matrix c_{ij} reduces to nine:

$$\begin{pmatrix} c_{11} & c_{12} & c_{13} & 0 & 0 & 0 \\ c_{12} & c_{22} & c_{23} & 0 & 0 & 0 \\ c_{13} & c_{23} & c_{33} & 0 & 0 & 0 \\ 0 & 0 & 0 & c_{44} & 0 & 0 \\ 0 & 0 & 0 & 0 & c_{55} & 0 \\ 0 & 0 & 0 & 0 & 0 & c_{66} \end{pmatrix}.$$

In this case eigenvalues of rheological matrixes $\mathbf{A}_x$, $\mathbf{A}_y$, $\mathbf{A}_z$ have a simple representation. For example, eigenvalues of matrix $\mathbf{A}_x$:

$$\mathbf{A}_x = -\begin{pmatrix} 0 & 0 & 0 & 1/\rho & 0 & 0 & 0 & 0 & 0 \\ 0 & 0 & 0 & 0 & 1/\rho & 0 & 0 & 0 & 0 \\ 0 & 0 & 0 & 0 & 0 & 1/\rho & 0 & 0 & 0 \\ c_{11} & 0 & 0 & 0 & 0 & 0 & 0 & 0 & 0 \\ 0 & c_{66} & 0 & 0 & 0 & 0 & 0 & 0 & 0 \\ 0 & 0 & c_{55} & 0 & 0 & 0 & 0 & 0 & 0 \\ c_{12} & 0 & 0 & 0 & 0 & 0 & 0 & 0 & 0 \\ 0 & 0 & 0 & 0 & 0 & 0 & 0 & 0 & 0 \\ c_{13} & 0 & 0 & 0 & 0 & 0 & 0 & 0 & 0 \end{pmatrix},$$

can be represented as $\left\{0, 0, 0, \sqrt{c_{11}/\rho}, \sqrt{c_{55}/\rho}, \sqrt{c_{66}/\rho}, -\sqrt{c_{11}/\rho}, -\sqrt{c_{55}/\rho}, -\sqrt{c_{66}/\rho}\right\}$. These eigenvalues also have a simple physical meaning. The eigenvalue $\sqrt{c_{11}/\rho}$ is equal to the speed of

the longitudinal wave front along the first axis. Eigenvalues $\sqrt{c_{55}/\rho}$ and $\sqrt{c_{66}/\rho}$ are equal to speeds of shear wave fronts, propagating along the first axis and having instantaneous speeds in directions of the second and the third axes.

3. GRID-CHARACTERISTIC NUMERICAL METHOD

3.1. Splitting by Spatial Directions

The solution of (2) can be obtained by using the partial steps method [20]. The original system (2) is splitted in three parts:

$$\frac{\partial \vec{u}}{\partial t} + \mathbf{A}_q \frac{\partial \vec{u}}{\partial q} = 0, \tag{3}$$

where $q = (x, y, z)$. For the equation (3) the relation f between the unknown vector on the next time layer $\vec{u}^{n+1}$ and on the current time layer $\vec{u}^n$ can be written as $\vec{u}^{n+1} = f_q(\mathbf{A}_q)\vec{u}^n$, where $q = (x, y, z)$. A similar relation for the equation (2) is written as

$$\vec{u}^{n+1} = F(\mathbf{A}_x, \mathbf{A}_y, \mathbf{A}_z)\vec{u}^n, \quad F(\mathbf{A}_x, \mathbf{A}_y, \mathbf{A}_z) = \alpha_x f_x(\mathbf{A}_x/\alpha_x) + \alpha_y f_y(\mathbf{A}_y/\alpha_y) + \alpha_z f_z(\mathbf{A}_z/\alpha_z). \tag{4}$$

If f_x, f_y, f_z represent numerical methods that provide at least a first order of the spatial approximation for (3) and the following requirement is met: $\alpha_x + \alpha_y + \alpha_z = 1$, $\alpha_x, \alpha_y, \alpha_z > 0$, the formula (4) guarantees the first order of the spatial approximation [21].

The stability condition, setting a limitation of the time step τ:

$$\tau \le \max \tau_j = \min h / \max |\lambda_j^*| = \min(h\alpha_j)/\max|\lambda_j|,$$

where λ_j are eigenvalues $\mathbf{A}_x$, $\mathbf{A}_y$, $\mathbf{A}_z$.

If f_x, f_y, f_z represent numerical methods that provide at least a second order of the spatial approximation for (3) and the resulting formula for the three-dimensional problem is replaced by $F(\mathbf{A}_x, \mathbf{A}_y, \mathbf{A}_z) = f_x(\mathbf{A}_x) f_y(\mathbf{A}_y) f_z(\mathbf{A}_z)$. We obtain the second order of the spatial approximation for the solution of (2).

3.2. Solution of a One-Dimensional Problem

The article [19] shows that eigenvalues and eigenvectors for rheological matrixes for an elastic anisotropic medium can be obtained analytically. There are nine real eigenvalues for each matrix, and we can introduce Riemann invariants to reduce (3) to the system of nine independent linear equations.

The matrix $\mathbf{A_q}$ can be presented in the following form: $\mathbf{A} = \mathbf{\Omega}^{-1}\mathbf{\Lambda}\mathbf{\Omega}$, where $\mathbf{\Omega}$ is the matrix, composed of eigen rows of matrix $\mathbf{A_q}$, $\mathbf{\Lambda}$ is the diagonal matrix, composed from eigenvalues of matrix $\mathbf{A_q}$. Multiplying (3) with $\mathbf{\Omega}$:

$$\mathbf{\Omega}\frac{\partial \vec{u}}{\partial t} + \mathbf{\Lambda}\mathbf{\Omega}\frac{\partial \vec{u}}{\partial x} = 0.$$

In linear elastic case, components of matrix $\mathbf{\Omega}$ are independent from variables (x, t):

$$\frac{\partial(\mathbf{\Omega}\vec{u})}{\partial t} + \mathbf{\Lambda}\frac{\partial(\mathbf{\Omega}\vec{u})}{\partial x} = 0.$$

Introducing Riemann invariants as $\vec{r} = \mathbf{\Omega}\vec{u}$, we obtain the following equation:

$$\frac{\partial \vec{r}}{\partial t} + \mathbf{\Lambda}\frac{\partial \vec{r}}{\partial x} = 0.$$

Corresponding components of the Riemann invariants vector $\vec{r}$ are constant along the characteristic lines:

$$\frac{dx}{dt} = \lambda_k, \quad k = \overline{1, 9}. \tag{5}$$

Thus, to obtain the solution for the (3) equations system, we follow this procedure for all the nodes in the computational mesh:

(i) casting nine characteristics from the node on the current time layer to the previous time layer according to the formula (5);

(ii) finding points of intersection of characteristics with the previous time layer;

(iii) interpolating Riemann invariants on previous time layer in these points [22];

(iv) reconstructing the solution of (3) from Riemann invariants according to the following formula: $\vec{u} = \mathbf{\Omega^{-1}}\vec{r}$.

3.3. Borders and Contacts

For border nodes, the procedure, described in the previous section, encounters a problem. Three of nine characteristics fall from the computational grid, and we must set border conditions for them. In the current implementation of the GCM, we replace necessary equations in (3) with border conditions and solve the resulting system numerically. For example, in case of the fixed border we replace equations for velocity vector components with these three: $\vec{v} = \vec{0}$. In case of contact node we, primarily, construct a virtual node on the contacting plane [21], interpolating its values from neighboring nodes. Then we solve the system of 18 equations numerically. This system is composed by the same principle as for border nodes. Twelve equations are taken from systems (3) for the contacting and the virtual nodes. The other six come from a contact condition—undestructible adhesion, sliding, friction, etc.

The destructible contact is modelled as described in [12]. A contact node is modeled as adhesed until the force threshold is achieved on some time step. Then the adhesion in the node is considered to be destroyed, and the contact type in the node is considered to be friction on all the followitng time steps.

3.4. Destruction of Composites

The set of availaible failure criteria for composites was presented in [12]: Tsai–Hill, Tsai–Wu, Drucker–Prager, Hashin, Puck. All these criteria use almost the same set of strength parameters accessible for direct measurement: tensile and compressive strengh along and across the ply direction, shear strengh in planes normal and parallel to the ply direction. The Hashin criterion also introduces the layer bond strength that allows to consider the weaker adhesion between different plies in composite subpacket [23]. The Puck criterion uses a complex failure model that considers different local fracture direction and introduces four internal parameters enveloping the inclination [24]. These parameters can be measured in the experiment, but their values (even for quite common composites) are not availaible in open access.

Tsai–Hill, Tsai–Wu, Drucker–Prager are based on Mises criterion —they provide a single formula to make a solution, whether the node in destroyed on the current time step or not. The Hashin criterion distinguishes several destruction mechanisms and allows for a more detailed analysis of the failure pattern. The Puck criterion distinguishes the same mechanisms as the Hashin criterion, but also gives the direction of local fractures in each destructed node. Thus, as the main criterion in this work we chose the Hashin criterion.

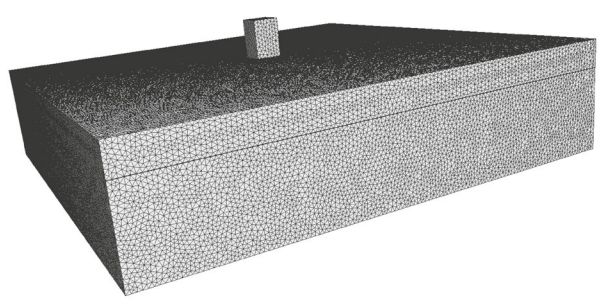

Fig. 1. General view of the computational domain, 2 mm titan layer.

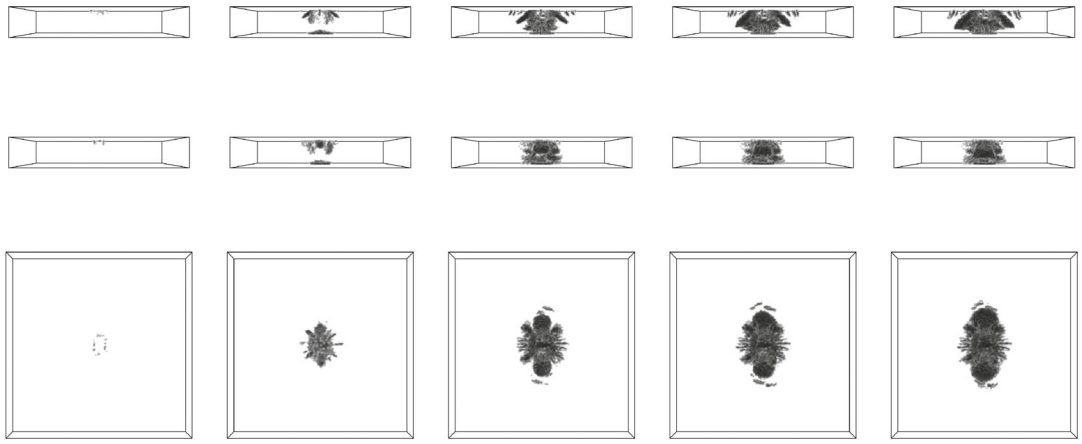

Fig. 2. Dynamic of destroyed area for CFRP without titanium. From left to right are consequent time steps. From top to bottom are axes X, Y, Z.

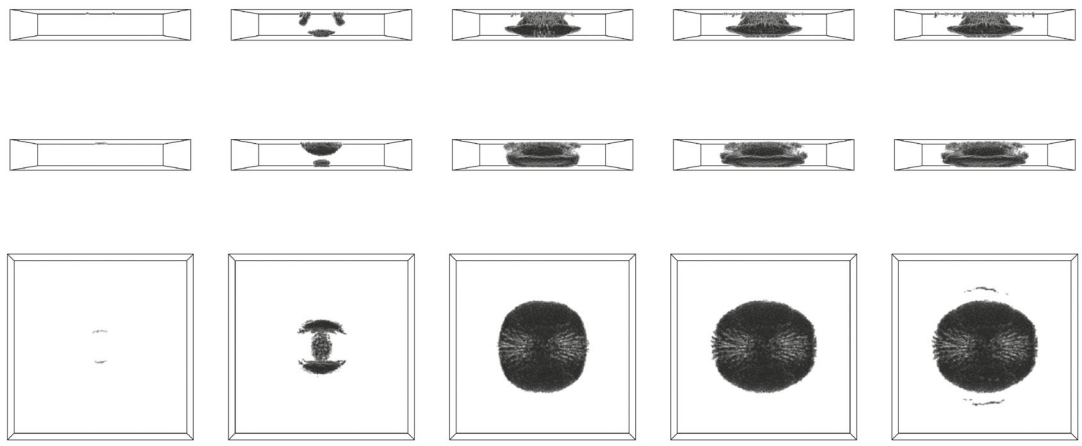

Fig. 3. Dynamic of destroyed area for CFRP with 1 mm titanium layer. From left to right are consequent time steps. From top to bottom are axes X, Y, Z.

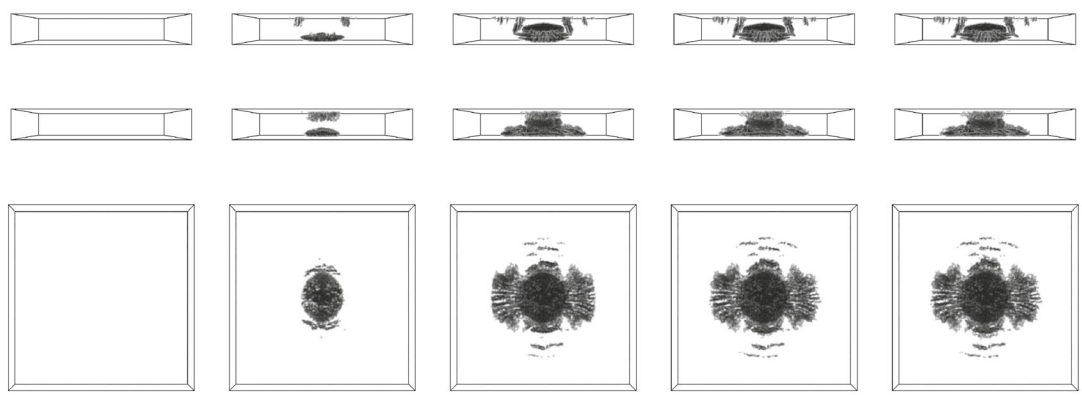

Fig. 4. Dynamic of destroyed area for CFRP with 2 mm titanium layer. From left to right are consequent time steps. From top to bottom are axes X, Y, Z.

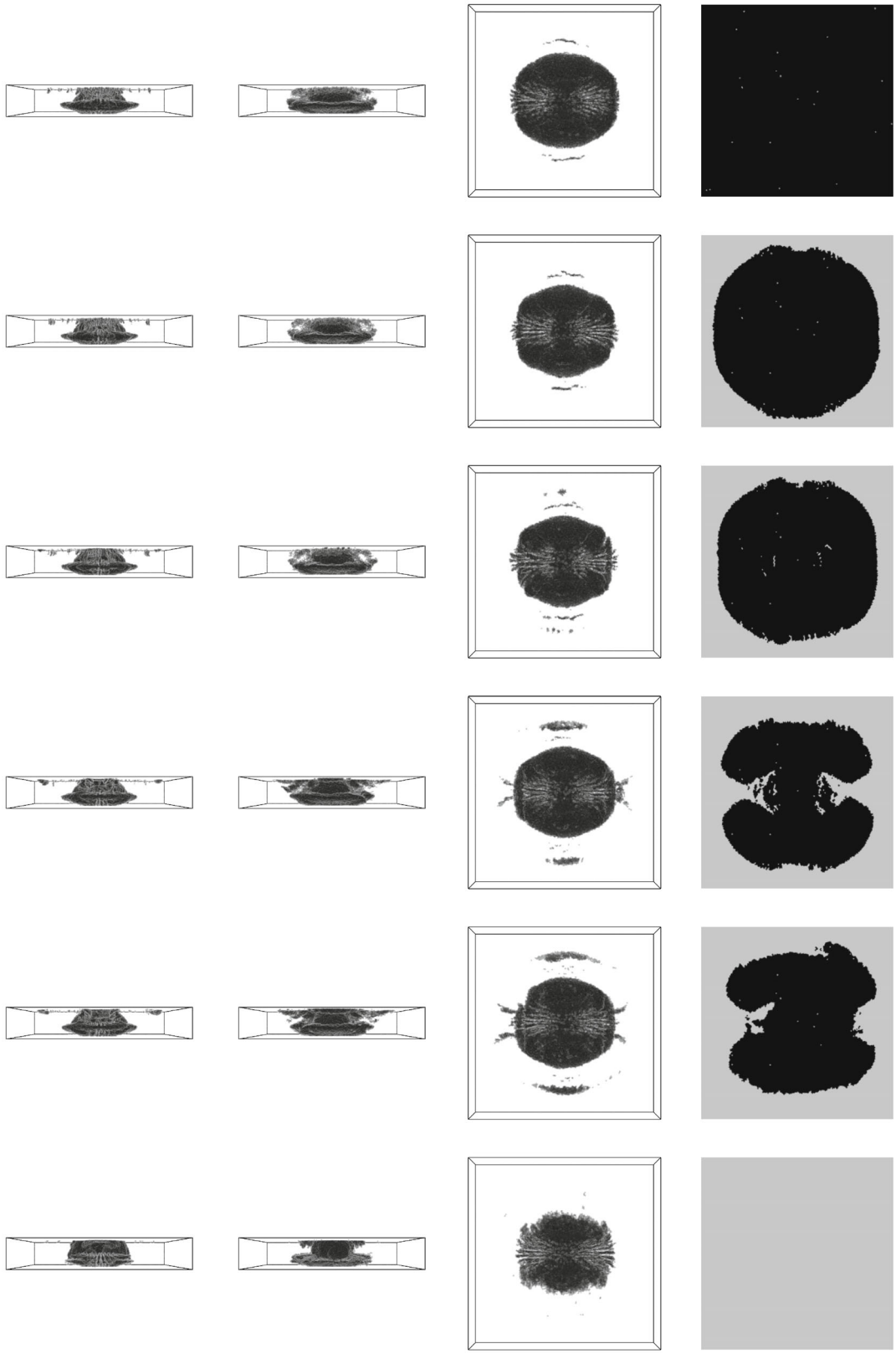

Fig. 5. Destroyed area, 1 mm titanium layer. From left to right are views from axes X, Y, Z and delamination between CFRP and titanium. From top to bottom are contact strength values 0, 0.6, 0.7, 0.8, 0.9, and 100 MPa.

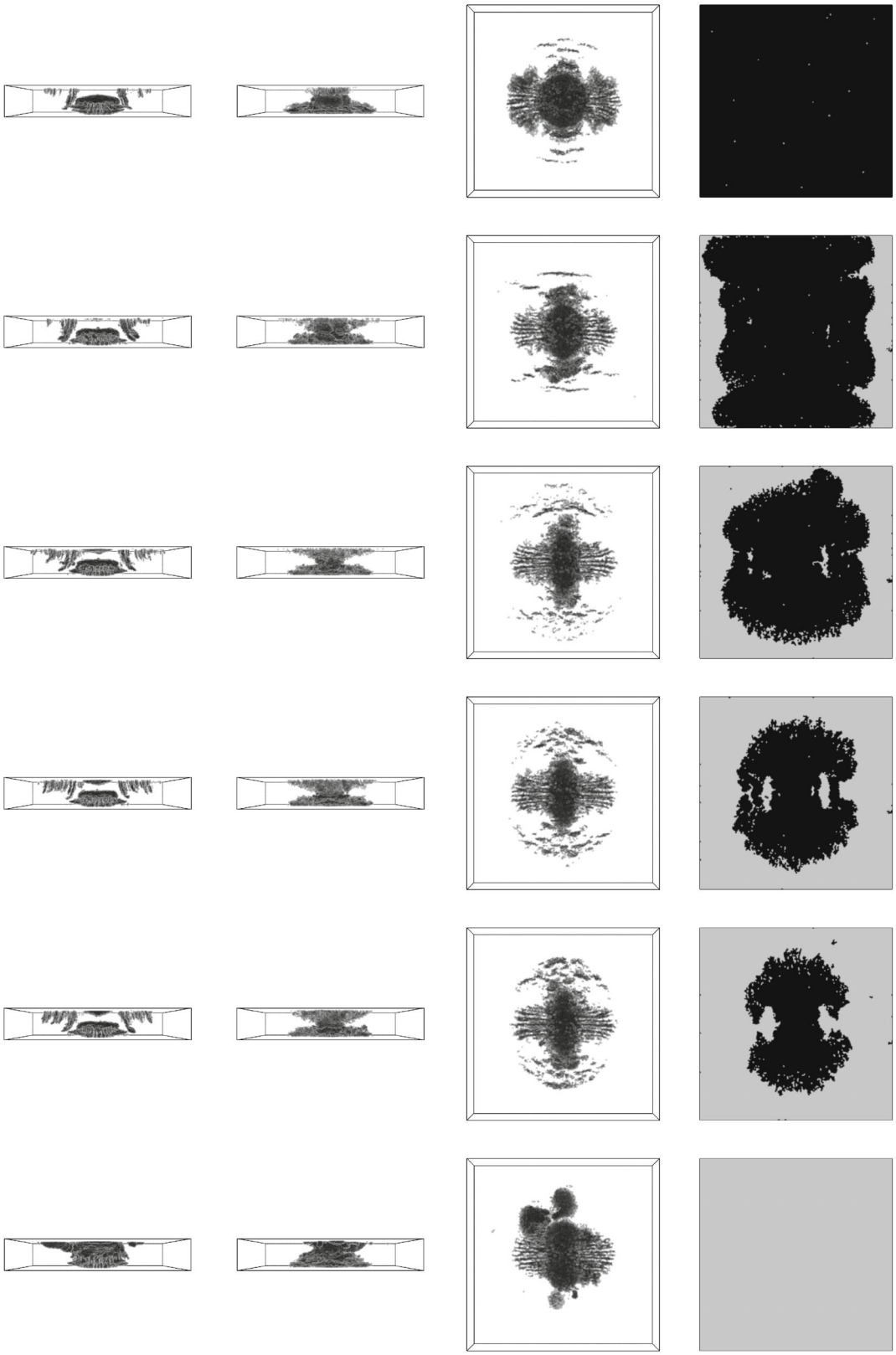

Fig. 6. Destroyed area, 2 mm titanium layer. From left to right are views from axes X, Y, Z and delamination between CFRP and titanium. From top to bottom are contact strength values 0, 0.6, 0.7, 0.8, 0.9, and 100 MPa.

4. LOW-VELOCITY IMPACT ON FIBER-METAL LAMINATE

4.1. Problem Statement

The general view of the computational domain is presented on Fig. 1. The fiber-metal laminate under consideration consists of a 6 mm carbon fiber reinforced polymer (CFRP) layer and titanium layer (1 or 2 mm). Energy of the small steel striker (12 mm^3) is 10 J. Layers of FML and striker are modeled as separate bodies with an explicit contact between them.

The size of the plate is 35 mm $\times$ 35 mm. It is enough to contain the whole destructed area for the chosen impact energy. Side borders are consuming. It effectively models an infinite bulk of the same material, which allows us to neglect the edge effects. Top and bottom borders are free.

The contact between striker and titanium layer is sliding without friction. The contact between titanium and CFRP is destructible, the contact strength was varied from 0 to 0.9 MPa (CFRP tension strength across the fiber direction is 0.86 MPa). The case of undestructible contact was also considered.

Steel properties are: density $\rho = 7800\ \mathrm{kg/m^3}$, Lame parameters are $\lambda = 104.4$ GPa, $\mu = 82$ GPa. Titanium properties are: density $\rho = 4500\ \mathrm{kg/m^3}$, Lame parameters are $\lambda = 120$ GPa, $\mu = 47$ GPa. Strengh and elastic properties of CFRP was taken from [17]. Metal destruction was not considered, because its strengh threshold is much higher than stresses in the low-velocity impact.

4.2. Numerical Results

The dynamic pattern of destroyed area for 1 mm titanium, 2 mm titanium and CFRP without titanium are presented on Figs. 2, 3, 4. CFRP-titanium contact strength in this case was 0 MPa.

The view from different axes allows to assess a complex three-dimensional form of the damaged area. Hashin criterion indicates that all the damage was caused by fractures in the epoxy and fibers were left intact.

The final destruction area for 2 mm titanium layer and different contact strength is presented on Figs. 5 and 6, including delamination.

Figures 5 and 6 show that the strength of contact influences both form and size of the destroyed area. While the dependency of the delamination size on the contact strength is quite obvious, the volume destruction pattern is more interesting. The presence of a titanium layer in this statement of the problem increases the destruction area. While the damage of pure CFRP is concentrated under the striker, other cases show a number of isolated cracks directly beneath the titanium layer. These cracks are parallel to the fiber direction. For 2 mm titanium layer these cracks are mostly small and multiple, but for a 1 mm titanium layer these cracks are larger and less numerous.

The size of damaged area is much larger than the size of the striker, but there are no significant and visible deformations on surfaces of the plate. It meets the conditions of BVID. The answer to a quiestion how does this damage influence the residual strength of the material requires an additional research.

5. CONCLUSIONS

The article contains the brief description of the grid-characteristic method for elastic anisotropic deformable bodies and numerical results that were obtained for model problems of a low-velocity impact on titanium composite laminates.

Fiber-metal laminates with titanium layers of 1 and 2 mm width were considered and compared with carbon fiber reinforced polymer without titanium layer. Different strength of contact between CFRP and metal were considered. Dynamic pattern of damaged area is presented.

The application of GCM for low-velocity impact problems can help to explain the damage pattern in composites, including delamination effects, by modelling elastic wave processes in the complex anisotropic medium.

ACKNOWLEDGMENTS

The research was supported by the Russian Science Foundation grant no. 17-71-10240.

REFERENCES

1. S. Abrate, "Impact on laminated composite materials," Appl. Mech. Rev. **44**, 155–190 (1991).
2. M. O. W. Richardson and M. J. Wisheart, "Review of low-velocity impact properties of composite materials," Composites, Part A **29**, 1123–1131 (1996).
3. S. Abrate, "Impact on laminated composites: recent advances," Appl. Mech. Rev. **47**, 517–544 (1994).
4. W. J. Cantwell and J. Morton, "The impact resistance of composite materials—a review," Composites **22**, 347–362 (1991).
5. P. Robinson and G. A. O. Davies, "Impactor mass and specimen geometry effects in low velocity impact of laminated composites," Int. J. Impact Eng. **12**, 189–207 (1992).
6. D. Delfosse and A. Poursatip, "Energy-based approach to impact damage in CFRP laminates," Composites **28**, 647–655 (1997).
7. A. Vlot, *Low-Velocity Impact Loading on Fibre Reinforced Aluminium Laminates (ARALL) and Other Aircraft Sheet Materials* (Tech. Univ. Delft, Delft, The Netherlands, 1991).
8. G. B. Chai and P. Manikandan, "Low velocity impact response of fibre-metal laminates—a review," Compos. Struct. **107**, 363–381 (2014).
9. M. Sadighi, R. C. Alderliesten, and R. Benedictus, "Impact resistance of fiber-metal laminates: a review," Int. J. Impact Eng. **49**, 77–90 (2012).
10. M. J. Hinton, A. S. Kaddour, and P. D. Soden, *Failure Criteria in Fibre Reinforced Polymer Composites: The World-Wide Failure Exercise* (Elsevier, Amsterdam, London, 2004).
11. M. J. Hinton and A. S. Kaddour, "Maturity of 3D failure criteria for fibre-reinforced composites: comparison between theories and experiments: Part B of WWFE-II," J. Compos. Mater. **7**, 925–966 (2013).
12. K. A. Beklemysheva, A. S. Ermakov, I. B. Petrov, and A. V. Vasyukov, "Numerical simulation of the failure of composite materials by using the grid-characteristic method," Math. Models Comput. Simul. **8**, 557–567 (2016).
13. I. B. Petrov and N. I. Khokhlov, "Modeling 3D seismic problems using high-performance computer systems," Math. Models Comput. Simul. **6**, 342–350 (2014).
14. K. A. Beklemysheva, A. A. Danilov, I. B. Petrov, V. Yu. Salamatova, Yu. V. Vassilevski, and A. V. Vasyukov, "Virtual blunt injury of human thorax: age-dependent response of vascular system," Russ. J. Numer. Anal. Math. Model **30**, 259–268 (2015).
15. I. B. Petrov and F. B. Chelnokov, "Numerical analysis of wave processes and fracture in layered targets," Comput. Math. Math. Phys. **43**, 1503–1519 (2003).
16. I. B. Petrov, A. V. Favorskaya, N. I. Khokhlov, V. A. Miryakha, A. V. Sannikov, and V. I. Golubev, "Monitoring the state of the moving train by use of high performance systems and modern computation methods," Math. Models Comput. Simul. **7**, 51–61 (2015).
17. N. Hu, Y. Zemba, T. Okabe, C. Yan, H. Fukunaga, and A. Elmarakbi, "A new cohesive model for simulating delamination propagation in composite laminates under transverse loads," Mech. Mater. **40**, 920–935 (2008).
18. I. B. Petrov, A. V. Favorskaya, A. V. Vasyukov, A. S. Ermakov, K. A. Beklemysheva, A. O. Kazakov, and A. V. Novikov, "Numerical simulation of wave propagation in anisotropic media," Dokl. Math. **30**, 778–780 (2015).
19. A. V. Favorskaya, "Statement of the problem of numerical simulation of dynamic processes in a continuous linearly elastic medium with anisotropy by the grid-characteristic method," in *Proceedings of the 54th Scientific MIPT Conference on Problems in Fundamental and Applied Sciences in Modern Information Environment* (2011), Vol. 2, pp. 55–56.
20. R. P. Fedorenko *Introduction to the Numerical Physics* (MIPT, Moscow, 1994) [in Russian].
21. F. B. Chelnokov, "Explicit representation of grid-characteristic schemes for the elasticity equations in two-dimensional and three-dimensional spaces," Mat. Model. **18** (6), 96–108 (2006).
22. I. B. Petrov and A. V. Favorskaya, "High-order interpolation on unstructured triangular and tetrahedral grids library," Inform. Tekhnol. **9**, 30–32 (2011).
23. Z. Hashin and A. Rotem, "Fatigue failure criterion for fiber-reinforced materials," J. Compos. Mater. **7**, 448–464 (1973).
24. A. Puck and H. Schurmann, "Failure analysis of FRP laminates by means of physically based phenomenological models," Compos. Sci. Technol. **62**, 1633–1662 (2002).